Model Verification of a Satellite with Large Flexible Appendages for Control System Design

Mooij, E.; Gransden, Derek I.

DOI
10.2514/6.2018-0209

Publication date
2018

Document Version
Accepted author manuscript

Published in
AIAA Guidance, Navigation, and Control

AIAA-18-0209

Model Verification of a Satellite with Large Flexible Appendages for Control System Design

E. Mooij and D.I. Gransden
Delft University of Technology, Delft, The Netherlands

AIAA Guidance, Navigation, and Control Conference
January 8-12, Kissimmee, FL

Model Verification of a Satellite with Large Flexible Appendages for Control System Design

Erwin Mooij* and Derek I. Gransden†

Delft University of Technology, Faculty of Aerospace Engineering,

Kluyverweg 1, 2629 HS Delft, The Netherlands

Power requirements of modern spacecraft compel large solar panels to fulfil functional needs without resorting to, for example, nuclear systems. It is common practice to develop a rigid-body control system to effect changes to the system state, that is, to manoeuvre and re-orient the spacecraft, without considering solar panel flexible body mechanics. The paper examines and compares the performance of a simple adaptive controller (SAC) and a linear quadratic reguluator (LQR) controller for their ability to control the flexible motion of the solar panels with respect to manoeuvring operations and a potential impact scenario. First the controller designs are explained, with details regarding the design of the SAC and how it computes the reference model to compare the difference of the plant state and commanded state. The linear three-dimensional structural beam model of the flexible appendages is explained including the time integration, which is performed through Newmark's method. Some verification studies are performed: comparisons between a commercial solver and the linear beam model are detailed, followed by a thorough investigation of the performance of the SAC with respect to an LQR controller. Monte-Carlo simulations provide a range of controller performance indices, which show that while the LQR can outperform the unoptimised SAC, the SAC is more robust in controlling oscillatory behaviour around the y-axis. Furthermore, with Monte-Carlo design optimisation, enabled by the rapid solution of the flexible mechanics, the SAC can be improved to be competitive with the LQR, and to exceed the performance of the LQR in control effort and oscillatory behaviour, in particular with the pitch and yaw thrusters.

I. Introduction

Satellites that have missions at relative large distance from the Sun require large solar panels to fulfil the power requirements without resorting to, for instance, nuclear means (Fig. 1). These solar panels have a significant impact on the mass properties of the complete satellite and their flexibility interacts with the dynamics of the system. However, smaller (and much lighter) satellites may also have large power demands. A good example is the category of communications satellites, with, for instance, panel lengths of about 19 m for the next generation of Intelsat satellites (Intelsat 29e, launched early 2016, spans a total of 44 m), or the total deployed length of 40.9 m of the HS-702 satellite bus of Hughes Space and Communications Company. In addition, the perturbing environment around Earth may be more demanding on the attitude control system, inducing a stronger interaction between flexible and rigid-body dynamics.

Previous research[1,2,3] focussed on the reorientation and associated attitude control of a rigid satellite with two large, flexible solar panels, for which the complex attitude control system has been based on a simple adaptive control algorithm. The rigid body-elastic body coupling in the simulation has been investigated using a finite element description with Lagrange multipliers as force constraints. The coupled dynamics of flexible and rigid bodies was observed to affect the efficacy and accuracy of the on-board controller. Due to the high gains and its model-following properties, the controlled response of the system approached that of a

*Assistant Professor, Section Astrodynamics and Space Missions, e.mooij@tudelft.nl, Associate Fellow AIAA.

†Assistant Professor, Section Structural Integrity & Composites, d.i.gransden@tudelft.nl.

Figure 1. Artist impression of Rosetta approaching comet 67P/Churyumov-Gerasimenko. Image: ESA

rigid body, albeit at the expense of a significant control effort. The complexity of this model and its associated computational cost prevents an extensive tuning of the adaptive controller, leading to a sub-optimal design.

To support control-system design and to allow for extensive controllability analysis, the existing flexible modeling is reviewed in terms of accuracy and simulation speed. For the current research, a simplified, linearised model will be developed, and compared and verified with a commercial FEM code. In terms of controller design, two principally different systems will be analysed, *i.e.,* a simple state-feedback controller with optimal gains (a so-called linear quadratic regulator) and the aforementioned simple adaptive controller. It is stressed that neither controller will be optimised for performance. The current study is merely aimed at setting up an efficient methodology with which controllers for (space) systems with flexibility can be designed and analysed. Nonetheless, the controller performances will be compared and suggestions for improvement given.

The remainder of this paper is organised as follows: Section II provides, after a brief background on simple adaptive control, a detailed overview of the control-system design and the benchmark results for a rigid satellite. Section III continues with a discussion on the theory and modelling aspects of flexible solar panels. In Sec. IV, the developed structural model and associated simulator is verified, and the results for a number of characteristic cases are given in Sec. V. Section VI concludes the paper and provides some recommendations.

II. Control System Design

A. Simple Adaptive Control

The attitude-control system is developed using the concept of so-called simple adaptive control (SAC),[4] and is based on the principle of tracking the output of a reference model. Therefore, this system could also be classified as a model reference adaptive control (MRAC) system, although a principal difference from the original MRAC is that full state knowledge of the plant to be controlled is not required. A schematic overview of a simple adaptive controller is shown in Fig. 2. The control law is given by

$$\mathbf{u_p}(t) = \mathbf{K_r}(t)\mathbf{r}(t) \tag{1}$$

where $\mathbf{r}(t) = [\mathbf{e_y}(t)\ \mathbf{x_m}(t)\ \mathbf{u_m}]^\mathsf{T}$ and $\mathbf{K_r}(t) = [\mathbf{K_e}(t)\ \mathbf{K_x}(t)\ \mathbf{K_u}(t)]$. It can be seen that the model input $\mathbf{u_m}$ and model state $\mathbf{x_m}$ are required to form part of the input signal $\mathbf{u_p}$ to the plant. Moreover, the so-called output error $\mathbf{e_y}$ serves as a feedback quantity to form the third element that composes $\mathbf{u_p}$. The three gains, *i.e.,* $\mathbf{K_x}$, $\mathbf{K_u}$ and $\mathbf{K_e}$, are adaptive.

To compute the adaptive gains, $\mathbf{K_r}$ is defined to be the sum of an integral and a proportional component:

$$\mathbf{K_r}(t) = \mathbf{K_i}(t) + \mathbf{K_p}(t) \tag{2}$$

with

$$\dot{\mathbf{K}}_\mathbf{i}(t) = \mathbf{e_y}\mathbf{r}^\mathsf{T}(t)\mathbf{T_i} \tag{3}$$

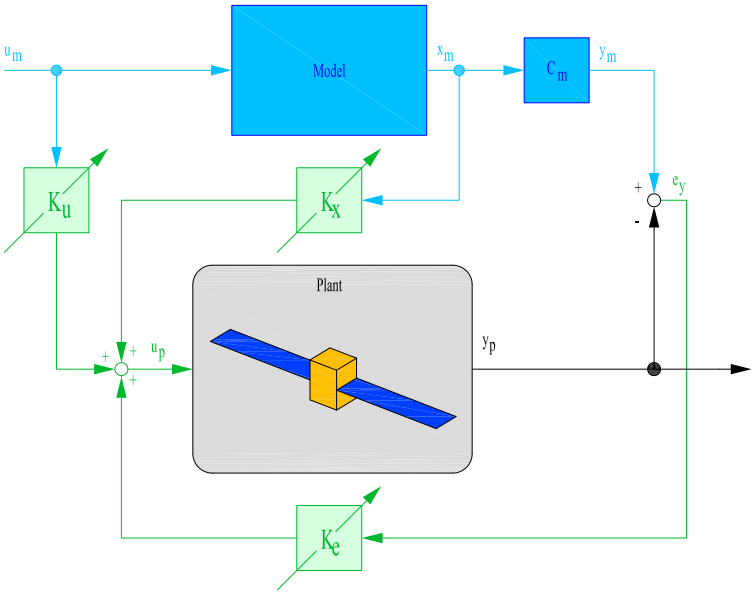

Figure 2. Basic architecture of a Simple Adaptive Control algorithm.

$$\mathbf{K_p}(t) = \mathbf{e_y}(t)\mathbf{r}^\mathsf{T}(t)\mathbf{T_p} \tag{4}$$

In Eqs. (3)-(4), the weighting matrices $\mathbf{T_p}$ and $\mathbf{T_i}$ are positive semi-definite and positive definite, respectively. Note that the proportional-gain component has a direct influence on the transient tracking behaviour, but is strictly speaking not required to enforce asymptotic tracking, as $\mathbf{T_p}$ can be zero. This is guaranteed by the integral gain. To improve the transient response by only using an integral gain, a constant gain value can be added to $\mathbf{K_i}$. An advantage over the use of the proportional gain is that this constant value is independent of $\mathbf{e_y}$, and is therefore non-zero even if $\mathbf{e_y}$ is zero. In that case, the integral gain derived from Eq. (3) becomes

$$\mathbf{K_i}(t) = \mathbf{K_{i,0}} + \int_0^t \dot{\mathbf{K}}_\mathbf{i}(t)\mathrm{d}t \tag{5}$$

One way to improve the damping of the system is to include the error derivatives in the output error vector. In that case, the error for output $\mathbf{y}$ becomes:

$$\mathbf{e_y}(t) = \mathbf{K_y^\mathsf{T}}(\mathbf{y_m}(t) - \mathbf{y_p}(t)) + \mathbf{K_{\dot{y}}^\mathsf{T}}(\dot{\mathbf{y}}_\mathbf{m}(t) - \dot{\mathbf{y}}_\mathbf{p}(t)) \tag{6}$$

with $\mathbf{K_y^\mathsf{T}}$ and $\mathbf{K_{\dot{y}}^\mathsf{T}}$ being a proportional and derivative output gain, respectively. However, to avoid calculating the numerical derivative of the outputs and to tune the related gains in multiple-output systems, an alternative expression for the output error may be used. Adjusting the output matrix by pre-multiplying it with $\mathbf{K_c}$, the optimal gain matrix from solving the Algebraic Riccati Equation for a closed-loop linearised version of the plant, sufficient damping is commonly introduced in the system to have a proper response.[5] The output error becomes in that case

$$\mathbf{e_y} = \mathbf{y_m} - \mathbf{y_p} = \mathbf{K_c}\left(\mathbf{C_m}\mathbf{x_m}(t) - \mathbf{C_p}(\mathbf{x_p}, t)\mathbf{x_p}(t)\right) \tag{7}$$

So far, an ideal environment has been considered. To cope with environmental disturbances that lead to a persistent non-zero error and therefore to a continuous change in the integral gain $\mathbf{K_i}$, a robust design can be applied to adjust the integral gain and prevent it from reaching very high values. The integral term of Eq. (3) is adjusted as follows:

$$\dot{\mathbf{K}}_\mathbf{i} = \mathbf{e_y}(t)\mathbf{r}^\mathsf{T}\mathbf{T_i} - \sigma_i\mathbf{K_i}(t) \tag{8}$$

Without the σ_i-term, $\mathbf{K_i}(t)$ is a perfect integrator and may steadily increase (and even diverge) whenever perfect output-following is not possible. Including the σ_i-term, $\mathbf{K_i}(t)$ is obtained from a first-order filtering of $\mathbf{e_y}(t)\mathbf{r}^\mathsf{T}\mathbf{T_i}$ and, therefore, cannot diverge, unless the output error diverges.

B. Reference Model

The current application of SAC focuses on a satellite with two large solar panels,[1,3] and has been schematically depicted in Fig. 3. Whereas an actual satellite consists of a rigid bus with two flexible solar panels, the reference model for the controller is assumed to be a linearised, rigid satellite. This choice should make it possible to obtain a more or less rigid-body response for an actual satellite if strict model following is achieved.

The geometry and mass properties of the rigid satellite have been defined such that they match those of a Rosetta-like satellite.[3] The satellite body is a parallelepiped with a height of 2.8 m, and a rectangular top and bottom cover of 2.1 m × 2.0 m. The mass of this body is 2,030 kg (dry mass plus current fuel; fuel sloshing is not considered, though), assumed to be uniformly distributed, with a corresponding inertia tensor of $\mathbf{I_{bus}} = \text{diag}(1991,1924,1364)$ kg m^2. The two solar panels are represented by rectangular flat plates of 14 m × 2.3 m, each having a mass of 40 kg and an inertia tensor of $\mathbf{I_{panel}} = \text{diag}(18,653,671)$ kg m^2, referenced to the panel centre of mass, which is located at half the panel length[a]. In the current simulation model, the panels are fixed to the satellite body with a stiff connection of 1 m, transferring forces and moments at a point on the related wall, located halfway down the satellite bus. The inertia tensor for the complete (rigid) system is $\mathbf{I_B} = \text{diag}(2027,9746,9150)$ kg m^2. The satellite's position is currently of no importance as neither the flight environment nor any coupling with the orbital motion is considered. Actuators for this satellite include a set of reaction control system (RCS) thrusters, with maximum available moments of $M_T = \pm 50$ Nm around each axis.

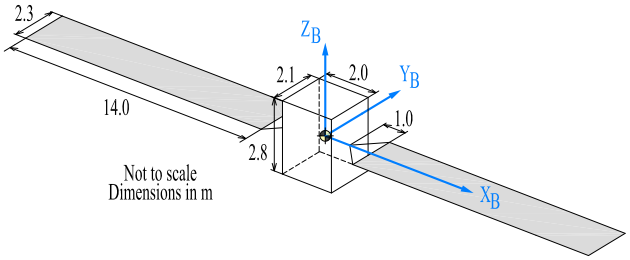

Figure 3. Satellite Geometry.

The reference model consists of a linearised state-space model for the rotational motion of the satellite, based on Euler angles for the attitude representation[b], *i.e.*,

$$\dot{\mathbf{x}}_\mathbf{m} = \mathbf{A_m x_m}(t) + \mathbf{B_m u_m}(t) \qquad \mathbf{y_m} = \mathbf{C_m x_m}(t) \tag{9}$$

with the model state and control vector given by

$$\mathbf{x_m} = \begin{pmatrix} p_m & q_m & r_m & \phi_m & \theta_m & \psi_m \end{pmatrix}^\mathsf{T} \qquad \mathbf{u_m} = \begin{pmatrix} M_{Tm,x} & M_{Tm,y} & M_{Tm,z} \end{pmatrix}^\mathsf{T}$$

and the model output vector $\mathbf{y_m}$ defined by the reference-model related part of Eq. (7), *i.e.*, $\mathbf{y_m} = \mathbf{K_c C_m x_m}(t)$. The above satellite model is stabilised by means of a linear quadratic regulator (LQR), *i.e.*, a linear state-feedback controller for which the gains, $\mathbf{K_c}$, have been computed with optimal control theory.[6] Input for the design of the LQR is the maximum allowable state deviation and the maximum control effort. The applied numerical values are $\Delta p_{max} = \Delta q_{max} = \Delta r_{max} = 0.2°/\text{s}$ and $\Delta\phi_{max} = \Delta\theta_{max} = \Delta\psi_{max} = 0.5°$ for the state variables, and $\Delta M_{Tx,max} = \Delta M_{Ty,max} = \Delta M_{Tz,max} = 50$ Nm for each of the control parameters. The low values for the angular-rate deviation should prevent actuator saturation, as the (heavy) satellite might be slow to start rotating. The small values for the angle deviations, on the other hand, would lead to slightly larger actuator commands such that the control will be "tighter". In terms of gain values, the ones associated with the angular rate carry more weight.

[a] The tensor is defined with respect to a local panel frame, with the X-axis pointing outwards along the panel centre line, the Y-axis parallel to the Y_B-axis, and the Z-axis being the right-handed complement.

[b] The definition of the Euler angles is the 3-2-1 definition commonly used in the aerospace industry. The time-rate of change is driven by the angular rate, representing the rotation of the body frame with respect to the inertial frame. The output of the controller is thus a moment vector in the body frame. To interface with the structural model that is inertial-frame referenced, appropriate transformation matrices are used to bring the control moment to the inertial frame, and, *vice versa*, the propagated (pseudo) Euler angles to the 3-2-1 definition.

C. Integrated System

The reference model is used in such a way that, when the commanded attitude changes, the effect is immediately noticeable to the model, and the closer the reference model approaches the commanded attitude, this effect will diminish. So rather than *following* the command, it will try to reduce the *difference* between plant state and command. For example, when a one-degree step is applied to any of the attitude angles, the corresponding model angle will develop a one-degree error that the stabilising LQR tries to reduce to zero. Since the corrective control will be large when faced with this error, it provides a strong reference signal to the adaptive controller. Any successive change in command will then be added as a differential error with respect to the previous command. The advantage of this implementation is that a maximum transient response is enforced right from the beginning, taking all information from the model into account. When the plant state approaches the commanded value, and the model has returned to its nominal state, the driving signal will be the output error, $\mathbf{e_y}$, and can be considered as a fine tuning of the response that removes the steady-state error. An additional advantage is that when in steady state, the input signals from the model are zero, and thus cannot result in jittering when a small output error occurs.

The design parameters of the adaptive controller are the weighting matrices, $\mathbf{T_p}$ and $\mathbf{T_i}$, the initial values of the integral gain, $\mathbf{K_{i,0}}$, and, as a safeguard against diverging output errors, the filter parameter, σ_i. Each of the attitude angles will be controlled separately, because the satellite under consideration is relatively heavy and slow to move and all three motion axes can be considered to be decoupled. This will simplify the controller design. Despite the large number of design parameters, one can relatively easily establish a baseline controller, and improve the performance by locally optimising the design. This can be done, for instance, by numerical optimisation or by trial and error, depending on the experience of the designer. Tables 1-3 list the values of the applied design parameters.

As an example of the satellite's response, commanded steps of $\phi_c = \psi_c = 1^\circ$ and $\theta_c = -1^\circ$ are executed at $t = 0$ s, where the satellite with its solar panels is treated as a single, rigid body, and the dynamics is evaluated using Euler's equation of rotational motion. Two simulations are done, *i.e.,* one with the LQR as stabilising controller for the nonlinear satellite, and one with SAC (with the same stabilising LQR included in the reference model). The results show that both the LQR and SAC provide a smooth and stable response. Figure 4 shows the time history of the three Euler angles obtained with the adaptive controller. For both ϕ and ψ it takes about 10 s to execute the command; the pitch response is a bit faster, even though this axis is the more difficult one to control. In the lower part of the figure, the corresponding control moments are plotted. As the controller is designed for accurate "pointing", allowing only small errors after a brief transient period, the thrusters are momentarily saturated. Once the satellite starts rotating, the thruster moments quickly reduce.

In Fig. 5 the control errors are shown, *i.e.,* the difference between the commanded and actual angles. The LQR is a bit faster in X and Z direction, whereas the SAC is faster in Y. From the preliminary test

Table 1. Design parameters roll controller

	T_p	T_i	$K_{i,0}$	σ_i
e_ϕ	10	15	80	0.2
p_m	10,000	20,000	100	0
ϕ_m	8,000	8,000	100	0
$M_{Tm,x}$	0.5	0.05	-1	0

Table 2. Design parameters pitch controller

	T_p	T_i	$K_{i,0}$	σ_i
e_θ	8	6	6	0.2
q_m	10,000	10,000	0	0
θ_m	8,000	8,000	0	0
$M_{Tm,y}$	0.005	0.01	0	0

Table 3. Design parameters yaw controller

	T_p	T_i	$K_{i,0}$	σ_i
e_ψ	10	15	100	0.2
r_m	10,000	20,000	2	0
ψ_m	8,000	8,000	2	0
$M_{Tm,z}$	0.05	0.03	-1.5	0

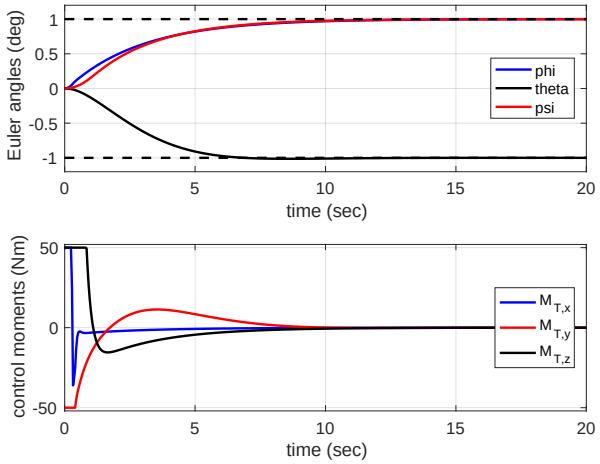

Figure 4. Rigid-body response for combined step commands (SAC).

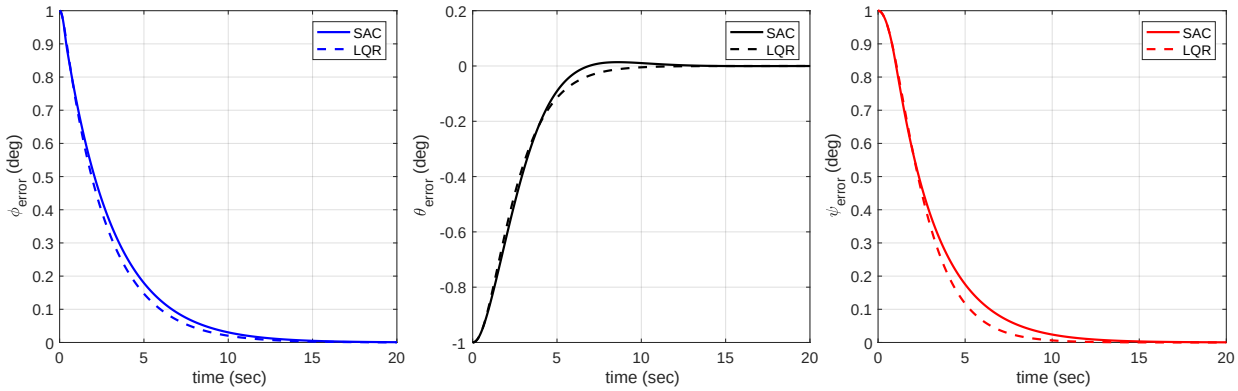

Figure 5. Control errors for both LQR and SAC (combined step commands).

results of the flexible-satellite response, it was found that θ is more difficult to control, so it is of interest to see what control errors occur once the flexible panels are included. Those results will be presented and discussed in Sec. V.

III. Satellite Structural Model

Work on articulated rigid body satellites with flexible multi-body appendages can be found, for instance, in Ref. 7, where the authors treat two different approaches: a Newtonian mechanics rigid body method and flexible motion treated with Lagrange equations and implemented with a finite element (plate) method. Stability analyses have also been performed for a rigid satellite bus coupled with solar arrays.[8] They show that flexible panels do influence the stability margins of the satellite, but the choice of modelling techniques may also influence its stability margins. Flexible solar arrays are commonly modelled as beams, or in a finite element software to determine the mode shapes, and applied to the state-space as normalised co-ordinates.[9,10,11]

In this work, the intention is to create a simplified structural model to replace the slower 3D hexahedral model with constrained rigid body and elastic body mechanics used in previous research,[2,3] which will be compared in a future paper. With a faster model, a comparison between a simplified linear model and a complex nonlinear model can be made to determine how the modelling technique influences the stability of the spacecraft. A computationally fast model with simplified geometry can be used to tune the adaptive controller and a more robust, more accurate but more computationally expensive, model can replace the

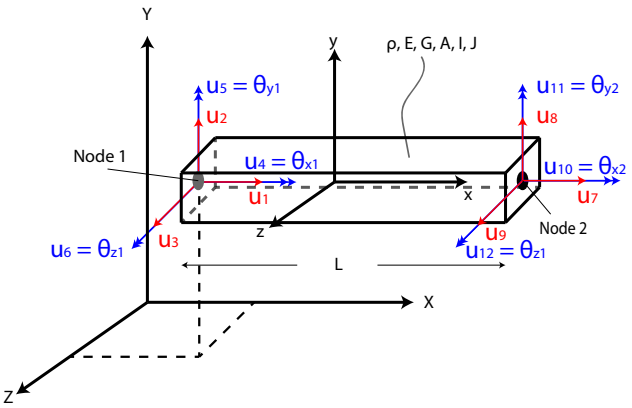

Figure 6. Beam Geometry.

simplified model when performing system-wide verification and validation.

Therefore, a linear, two node-per-element, three-dimensional Euler-Bernoulli beam model replaces the former to allow for fast sensitivity and controller verification with respect to variable geometric and material properties. The beam model is separated into three physical parts: the flexible solar panels, a rigid-like link that separates the solar panels from the satellite bus, and the satellite bus itself. The three parts are exactly as described in Ref. 3; Figure 3 shows the global co-ordinate system and satellite geometry. However, in place of the constrained mechanics of the previous work, a continuous beam model is presented such that the satellite bus and links are represented together, without the use of Lagrange multipliers that may destabilise the simulation.[12]

The beam model uses a set of Tait-Bryan angles as a directional cosine matrix for the orientation of the deformed beam. In the initial configuration, the beam model is coincidental with the inertial X-axis. Figure 6 shows a beam element with nodes 1 and 2, in the deformed configuration with respect to the inertial co-ordinate system. (Note: the directional rotation angles do not, in general, correspond to the Euler angles used for the controller. The transformation matrix is the multiplication of the rotation about the x-, y-, and z-axes.) Elemental positive directions are initially assumed to be co-linear with the inertial co-ordinate system.

Euler-Bernoulli beam models are common in finite element mechanics texts, although it is more difficult to find three-dimensional beam models. For a three-dimensional development of a beam model, a reader is referred to Refs. 13 and 14, as examples. To give an impression of the elemental mass and stiffness matrices, the matrices are presented in their full form in Eqs. (10) and (11) in the beam element local coordinate system:

$$\mathbf{m}_e = \rho AL \begin{bmatrix} \frac{1}{3} & 0 & 0 & 0 & 0 & 0 & \frac{1}{6} & 0 & 0 & 0 & 0 & 0 \\ & \frac{13}{35} & 0 & 0 & 0 & \frac{11L}{210} & 0 & \frac{9}{70} & 0 & 0 & 0 & -\frac{13L}{420} \\ & & \frac{13}{35} & 0 & -\frac{11L}{210} & 0 & 0 & 0 & \frac{9}{70} & 0 & \frac{13L}{420} & 0 \\ & & & \frac{I_y+I_z}{3A} & 0 & 0 & 0 & 0 & 0 & \frac{I_y+I_z}{6A} & 0 & 0 \\ & & & & \frac{L^2}{105} & 0 & 0 & 0 & -\frac{13AL}{420} & 0 & -\frac{L^2}{140} & 0 \\ & & & & & \frac{L^2}{105} & 0 & -\frac{13L}{420} & 0 & 0 & 0 & -\frac{L^2}{140} \\ & & & & & & \frac{1}{3} & 0 & 0 & 0 & 0 & 0 \\ & & & & & & & \frac{13}{35} & 0 & 0 & 0 & -\frac{11L}{210} \\ & & & & & & & & \frac{13}{35} & 0 & \frac{11L}{210} & 0 \\ & & & & & & & & & \frac{I_y+I_z}{3A} & 0 & 0 \\ & & & & & & & & & & \frac{L^2}{105} & 0 \\ \text{sym.} & & & & & & & & & & & \frac{L^2}{105} \end{bmatrix} \tag{10}$$

and

$$\mathbf{k}_e = \frac{E}{L}\begin{bmatrix} A & 0 & 0 & 0 & 0 & 0 & -A & 0 & 0 & 0 & 0 & 0 \\ & \frac{12I_z}{L^2} & 0 & 0 & 0 & \frac{6I_z}{L} & 0 & -\frac{12I_z}{L^2} & 0 & 0 & 0 & \frac{6I_z}{L} \\ & & \frac{12I_y}{L^2} & 0 & -\frac{6I_y}{L} & 0 & 0 & 0 & -\frac{12I_y}{L^2} & 0 & -\frac{6I_y}{L} & 0 \\ & & & \frac{GJ}{E} & 0 & 0 & 0 & 0 & 0 & -\frac{GJ}{E} & 0 & 0 \\ & & & & 4I_y & 0 & 0 & 0 & \frac{6I_y}{L} & 0 & 2I_y & 0 \\ & & & & & 4I_z & 0 & -\frac{6I_z}{L} & 0 & 0 & 0 & 2I_z \\ & & & & & & A & 0 & 0 & 0 & 0 & 0 \\ & & & & & & & \frac{12I_z}{L^2} & 0 & 0 & 0 & -\frac{6I_z}{L} \\ & & & & & & & & \frac{12I_y}{L^2} & 0 & \frac{6I_y}{L} & 0 \\ & & & & & & & & & \frac{GJ}{E} & 0 & 0 \\ & & & & & & & & & & 4I_y & 0 \\ \text{sym.} & & & & & & & & & & & 4I_z \end{bmatrix} \tag{11}$$

where L is the element length, which is a function of the positions of the element nodes. In these equations, E is the isotropic beam material Young's modulus, G is the material shear modulus, A is the beam cross-section area, I_y and I_z are the y- and z- second moments of area of the beam, J is its polar moment, and ρ is the density of the beam element. Here it must be re-iterated that the beam element properties depend on the location of the element with respect to the satellite, that is, the material and geometric properties listed are consistent with the part of the satellite upon which the element exists. In other words, E, G, A, I_y, I_z, J, and ρ depend on whether the element is part of the satellite bus, the connecting link, or the solar panels.

With the matrices from Eqs. (10) and (11), the global mass and stiffness matrices, $\mathbf{M}$ and $\mathbf{K}$, are assembled using the transformation

$$\mathbf{M} = \mathbf{R}^{\mathsf{T}}\mathbf{m}_e\mathbf{R} \tag{12}$$

$$\mathbf{K} = \mathbf{R}^{\mathsf{T}}\mathbf{k}_e\mathbf{R} \tag{13}$$

where

$$\mathbf{R} = \begin{bmatrix} \mathbf{r} & 0 & 0 & 0 \\ & \mathbf{r} & 0 & 0 \\ & & \mathbf{r} & 0 \\ \text{sym.} & & & \mathbf{r} \end{bmatrix} \tag{14}$$

and $\mathbf{r}$ is the product of the rotation matrices

$$\mathbf{r} = \mathbf{X}\left(\theta_x\right)\mathbf{Y}\left(\theta_y\right)\mathbf{Z}\left(\theta_z\right) \tag{15}$$

where $\mathbf{X}$, $\mathbf{Y}$, $\mathbf{Z}$ are intrinsic rotations. Therefore, once the nodal displacements have been calculated, the internal (elemental) forces and moments can be recovered as

$$\mathbf{F}_e = \mathbf{k}_e\mathbf{R}\mathbf{d}_e \tag{16}$$

The elemental force and displacement vectors are given as

$$\mathbf{F}_e = \begin{bmatrix} F_x^{(1)} & F_y^{(1)} & F_z^{(1)} & M_x^{(1)} & M_y^{(1)} & M_z^{(1)} & F_x^{(2)} & F_y^{(2)} & F_z^{(2)} & M_x^{(2)} & M_y^{(2)} & M_z^{(2)} \end{bmatrix}^{\mathsf{T}} \tag{17}$$

and

$$\mathbf{d}_e = \begin{bmatrix} x^{(1)} & y^{(1)} & z^{(1)} & \theta_x^{(1)} & \theta_y^{(1)} & \theta_z^{(1)} & x^{(2)} & y^{(2)} & z^{(2)} & \theta_x^{(2)} & \theta_y^{(2)} & \theta_z^{(2)} \end{bmatrix}^{\mathsf{T}} \tag{18}$$

where the superscript denotes the element nodal number.

These matrices are assembled in the same manner as the solid body elastic mechanics, which will have the generic form (since a damping ratio is not currently used):

$$\mathbf{M}\ddot{\mathbf{d}} + \mathbf{K}\mathbf{d} = \mathbf{F} \tag{19}$$

The time integration is done by Newmark's method, which allows one to have second-order accuracy for a spectral radius, $\rho_\infty = 1.0$, and is stable under the conditions

$$\gamma \geq \frac{1}{2}, \qquad \beta \geq \frac{1}{4}\left(\gamma + \frac{1}{2}\right)^2$$

So, for each time step one can rewrite Eq. (19) as

$$\mathbf{M}\mathbf{a}_{n+1} + \mathbf{K}\mathbf{d}_{n+1} = \mathbf{F}\left(t_{n+1}\right) \tag{20}$$

where according to Newmark's method, updating the acceleration and velocity is given by,

$$\left.\begin{aligned} \mathbf{a}_{n+1} &= \tfrac{1}{\beta\Delta t^2}\left(\mathbf{d}_{n+1} - \mathbf{d}_n\right) - \tfrac{1}{\beta\Delta t}\mathbf{v}_n - \tfrac{1-2\beta}{2\beta}\mathbf{a}_n \\ \mathbf{v}_{n+1} &= \mathbf{v}_n + \gamma\Delta t\mathbf{a}_{n+1} + \left(1-\gamma\right)\Delta t\mathbf{a}_n \end{aligned}\right\} \tag{21}$$

Now that all unknowns can be described using only the unknown displacements, $\mathbf{d}_{n+1}$, by taking the Gateaux derivative, and rearranging the terms so that the unknown displacements are on the left side of the equation,

$$\left\{\frac{1}{\beta\Delta t^2}\mathbf{M} + \mathbf{K}\right\}\mathbf{d}_{n+1} = \frac{1}{\beta\Delta t^2}\mathbf{M}\mathbf{d}_n + \frac{1}{\beta\Delta t}\mathbf{M}\mathbf{v}_n + \frac{1-2\beta}{2\beta}\mathbf{M}\mathbf{a}_n + \mathbf{F}\left(t_{n+1}\right) \tag{22}$$

$$\mathbf{K}_{\text{effdyn}}\mathbf{d}_{n+1} = \mathbf{F}_{\text{effdyn}}\left(t_{n+1}\right) \tag{23}$$

which is solved in the usual manner. With $\mathbf{d}_{n+1}$ known, one can solve for the unknown velocities and accelerations using Eq. (21).

IV. Flexible Satellite Verification

Before applying the beam model to various attitude-control problems, and discussing the results of the controllability analysis, the developed models and simulator are compared to a commerical model. This is done both from a structural and an operational point of view.

To verify the linear Euler-Bernoulli beam model, a beam model is implemented in Dassault Systèmes Abaqus®. Both models, which will be referred to as the simplified model and the commercial model, are created in the same manner: a connected set of elements representing the span of the satellite from the solar panels, the connecting link, and the satellite bus, with the appropriate symmetry. Both models have 80 elements spanning each of the solar panels, each rigid link has 1 element, and the satellite bus consists of 2 elements, for a total of 164 elements and 990 degrees of freedom.

Both models have the same geometric and material properties, as shown in Table 4. In this table the labels $\mathrm{m_{sp}}$, $\mathrm{m_{bus}}$, and $\mathrm{m_{link}}$ refer to the masses of each of the solar panels, the satellite bus, and each of the connecting links, respectively. The total mass of the satellite is given by $\mathrm{m_{tot}}$ and the mass moments of inertia I_{xx}, I_{yy}, and I_{zz} are also for the entire satellite. Both models' flexibility parameters are based upon an estimated 1 Hz cantilever-beam first natural frequency. The natural frequencies of both models are listed in Table 5.

Table 4. Mass properties of simplified model and commercial model

	$\mathrm{m_{tot}}$ kg	$\mathrm{m_{sp}}$ kg	$\mathrm{m_{bus}}$ kg	$\mathrm{m_{link}}$ kg	I_{xx} kgm^2	I_{yy} kgm^2	I_{zz} kgm^2
Simplified	2030	40	1950	0.1	2027	9746	9150
Commercial	2030	40	1950	0.1	2026	10036	9154

Table 5. Natural frequencies of the simplified model and commercial model

	1^{st}	2^{nd}	3^{rd}	4^{th}	5^{th}	6^{th}
Simplified [Hz]	1.029	2.653	6.395	7.858	17.86	18.79
Commercial [Hz]	1.029	1.925	6.394	6.867	17.86	18.12
% Difference	0.000	31.80	0.000	13.46	0.000	0.04

The differences in the natural frequencies can perhaps be explained by the default use of Timoshenko elements (B32 elements) in Abaqus, although with a correction for the slenderness ratio, and the fact that the commercial model uses fewer assumptions regarding the reduction in dimensionality of the physical system. (For example, in the simplified model shear effects are neglected and bending loads do not contribute to the extension or contraction of the beam.) It should be noted that the eigenmodes of the two models are identical for symmetric modes and vary slightly (a larger slope of the satellite bus orientation in the Abaqus model) in the anti-symmetric modes. Since the mass properties of the two models are nearly identical, varying by less than 3% in the case of I_{yy}, it seems the main contribution for the differences of the natural frequencies arises from the stiffnesses, and the stiffness of the Abaqus-generated model must be lower for anti-symmetric cases. The effective Young's moduli are chosen to be the same for each partition of the beam: the solar panels, the connecting links, and the satellite bus; therefore, this must come from the additional contributions of a more rigourous model in the commercial software. It would seem to support the fact that the rotations of the satellite hub in the anti-symmetric modes are due to shear effects that are not considered in the simplified model. (Additionally, the simplified model does not support large rotations, which limits the validity of the model.) These effects are also apparent on the displacement of the longitudinal co-ordinate.

The Newmark parameters used in the simplified model are based on $\rho_\infty = 1.0$, which means $\beta = 0.25$ and $\gamma = 0.5$, but the commercial model uses the defaults in the explicit-dynamic solver. There is a difference in the time step between the two models: the simplified model uses a $\Delta t = 0.002$ s (an order of magnitude lower than the nominal control simulations), but the commercial model automatically calculates the time step, which was found to be $\Delta t = 5 \times 10^{-8}$ s. The stable time increment in Abaqus is quite small due to the size of the elements and the wave speed of the material, and the fact that the solver is an explicit procedure. Due to the implicit nature of the Newmark method, a larger step size can be used. (Structural step size sensitivity was performed; a $\Delta t = 0.002$ s was concluded to be sufficient when compared to finer time discretisations.) Therefore, the computational time for both models is also not equivalent. To test the simplified model, and to connect the research with a paper related to orbital control with low-momentum impacts,[15] an impact of an object with the spacecraft is simulated. Both models (simplified and commercial) are run with an impact of 100 N, uncontrolled, in the z- and y-directions for a duration of 0.02 s and left to drift for the remaining time up to 10 s, at which time the simulation ends.

The results of the impact simulation on the two models show some differences, in particular in the starboard solar-panel edge displacement and velocity. These two indicators were chosen, because they give the greatest deviation from the rigid body deflections and are also closely related to the values the controller uses, which are the angles and angular velocities of the satellite bus. Figure 7 shows the tip displacements of the starboard solar-panel edge as a function of time and the rigid-body tip displacement is included to show what the rotational displacement would be in the case the stiffnesses were infinite. The final tip displacement is compared in Table 6, with the rigid tip displacement given as well. Clearly, the rigid tip displacement is not meant to be compared to the elastic body displacements; however, it is useful to see the effect of the rigidity of the panels, given that the moments of inertia are greater in the y-direction than in the z-direction.

Figure 7 shows that there is an approximately constant discrepancy between the simplified model and the commercial model, but otherwise the vibratory motion of the solar panels is reasonably well captured. For each direction, the same period and amplitude of elastic motion is found for the flexible bodies, although it is not clear for the y-direction. The x-axis displacement has a non-constant error due to the combined effect of the additional displacement of the y- and z-axes. Figure 8 shows the starboard edge velocity during the simulation time, and it is clear that the discrepancy in the displacement variables comes from the differences in velocity. While the commercial-solver edge velocities oscillate around the rigid-body velocities, the simplified model velocities are offset. This is particularly visible in v_y, in which high-frequency but small-amplitude vibrations dominate the elastic response. Table 6 summarises the differences between the end-time tip displacements of both models.

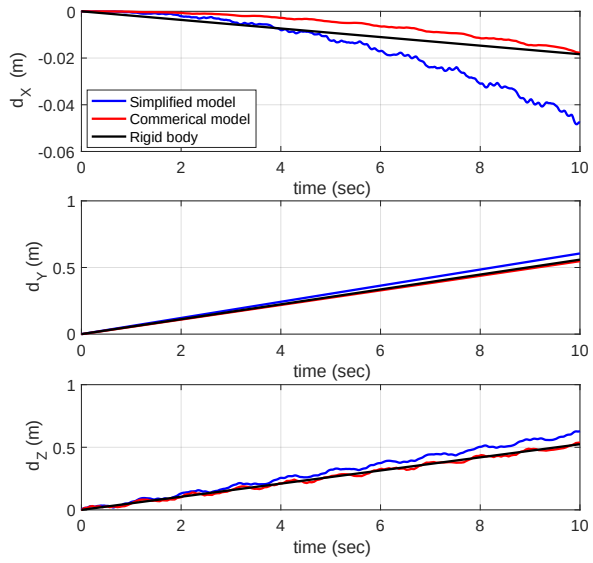

Figure 7. Starboard edge displacements of both models and rigid body motion during impact and drift phases of the simulation.

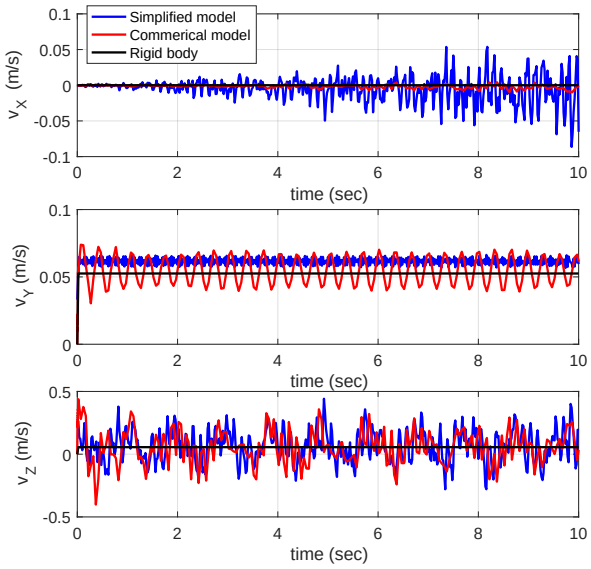

Figure 8. Starboard edge velocity of both models and rigid body motion during impact and drift phases of the simulation.

Table 6. Comparison of the tip displacement after 10 s of uncontrolled drift

	d_x	d_y	d_z
Simplified [Hz]	-0.0475	0.605	0.629
Abaqus [Hz]	-0.0177	0.547	0.537
% Difference	91.4	10.1	15.8

Despite the differences between the simplified model and the commercial software, it does indicate that the simplified model reasonably calculates displacements that are on the correct order and it is computationally cheaper than a full three-dimensional continuum or commercial software model. For the remaining verification simulations, the Newmark's method parameters are adjusted to include some minor damping, such that $\rho_\infty = 0.95$, $\beta = 0.263$, and $\gamma = 0.5256$. These parameters are chosen to reduce the undesirable numerical high frequency oscillations in the solution that cause the controller to over-correct and become unstable. Additionally, the time step, $\Delta t = 0.02$ s is used for the remaining simulations.

To exemplify the performance of the simplified flexible beam model coupled with the controller, a rotation of 1° about the body x- and z-axes, and a negative 1° about the body y-axis is performed. The controller operates at a frequency of 50 Hz, which will be explained later in this subsection. Figures 9 and 10 show the solar-panel edge displacement and velocities in the global (inertial) frame of reference. The response of the flexible bodies is controlled in under 10 s, after which the velocities of the tips are approximately zero.

Figure 11 shows the relative displacement of the panels with respect to the satellite bus, which is also rotating, at the time when the deformation in the z-direction is greatest. This occurs at $t = 0.18$ s. The δ_x, δ_y, and δ_z refer to the deformation displacement, which is the difference of the total displacement and the rigid body rotation. Figure 12 shows the time history of the deformation in the z-direction. The oscillations of the deformation are quickly counteracted by the controller, although there is a small steady-state error that corresponds to less than 10% the accepted pointing accuracy requirement.

The final verification step addresses some numerical issues. The simplified, flexible model will be compared against the rigid-satellite simulator that was developed earlier.[3] That model is non-linear using the Euler equations to describe the rotational dynamics, and in its current configuration the Runge-Kutta (RK) fourth-order integration method, such that the system can be considered to be a continuous system. The controllers are discretised and sampled at discrete times. The adaptive integral gains are propagated with finite-difference equations, equal to an Euler integration.

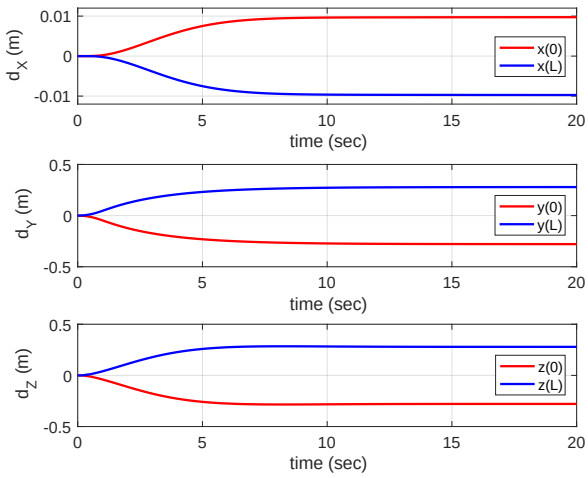

Figure 9. Global displacement of the port and starboard solar-panel edges.

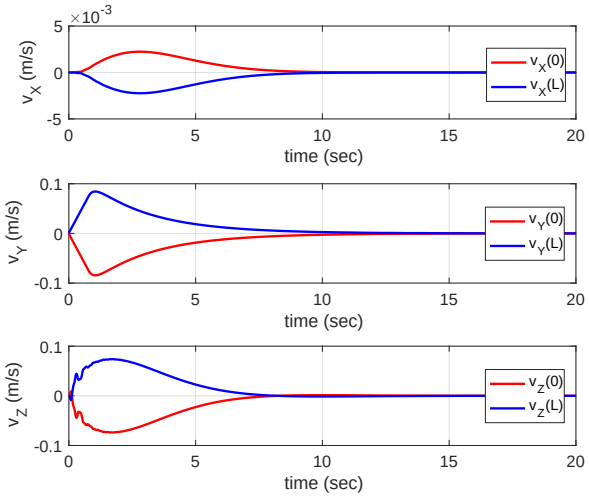

Figure 10. Velocity of the port and starboard solar-panel edges.

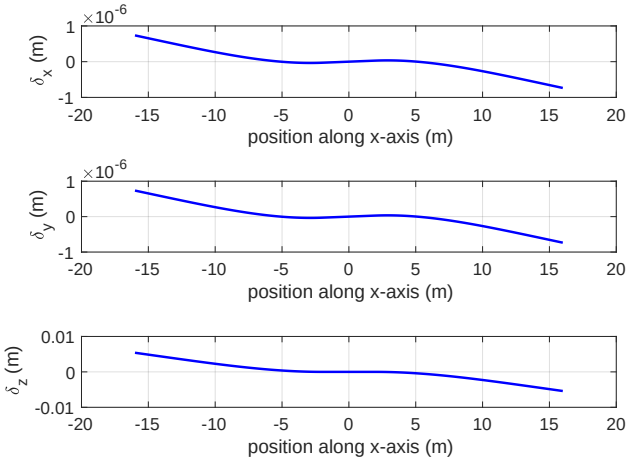

Figure 11. The relative deformation of the satellite with respect to the satellite hub.

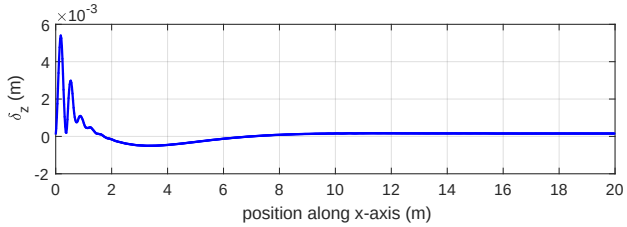

Figure 12. Starboard solar-panel edge deformation relative to the satellite bus.

The simplified, flexible model, on the other hand, is in total a discretised model, and propagated with Newmark's method, effectively a single time-step method. Also in this case, the controllers are discretised, which means that the complete system is based on two sequential single-step integrations. Whereas in the previous research the controllers operated at 25 Hz, in the current paper this frequency has been doubled to match the integration step size of the flexible model, simply to avoid (numerical) oscillatory behaviour that was observed at lower controller frequencies. Ongoing work is aimed at reprogramming the propagation of the structural model using a RK integrator.

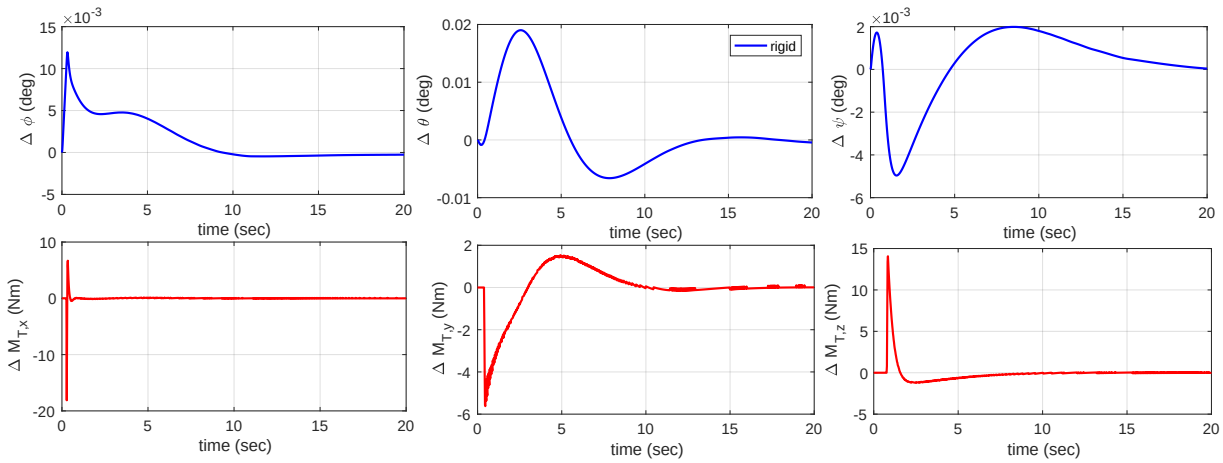

Figure 13. Verification: difference between the rigid and the stiff/flexible satellite (combined step commands).

To test the setup, the combined step commands are simulated both with the rigid-satellite and the flexible-satellite simulator, in combination with the adaptive controller. However, the flexible satellite has been made very stiff by multiplying the Young's modulus, E, and shear modulus, G, of satellite bus and panels with a factor of 100. In this way an approximated rigid satellite is obtained. Preliminary simulations showed, however, that there were some numerical issues especially related to ψ, which could not be removed by decreasing the step size and/or increasing the controller frequency. Lowering the number of structural elements from 80 to 10, reduced the "numerical stiffness" of the problem and a proper response was obtained.

In Fig. 13 the difference between the two responses for the Euler angles and the control moments are shown. The angle differences are small at all times and smoothly reduce to zero. The control moments show somewhat larger errors, or rather discrete jumps. However, these are easily explained by the nature of the response test. The commanded step functions require an almost instantaneous maximum control effort, because the controller is designed for accurate pointing. Even a shift of a single control sample (Δt = 0.02 s) will show as a large error. Inspecting the individual moment curves, though, shows an identical behaviour. Therefore, it can be concluded that in a limit configuration the flexible system behaves as a rigid body. It seems justified to state that this model can be used for controllability study on a variety of satellite configurations.

V. Results

This section presents the applicability of the developed simulation environment and contains the dual objective of performing controllability studies and/or to propose a (re-)design attitude controllers for satellites with flexible appendages. An extensive verification process confirming the applicability of the simulator was discussed in the previous Sec. IV. Section V.A provides some background on controller-performance analysis, which is successively done in the following Sec. V.B. Whereas in that section the focus is on controller robustness when the satellite properties change without changing the controller, Sec. V.C addresses the influence of controller design on the performance of a nominal satellite configuration.

A. Performance Analysis

The performance of a controller can be derived from several defined objective function(s). For the current control-system design, one may look at the minimum state deviation of the satellite (or the plant) with respect to the guidance commands.[c] Another objective in the design could be to minimise the control effort that is required to influence the plant's behaviour. For the current satellite-control problem, these two objectives can be expressed as the integrated Euler-angle deviation and the integrated thruster activity (the total amount of fuel, or, equivalently, the required control moments), given by:

[c]Besides the deviation from the command, the difference with respect to the corresponding reference-model state could also be used, assuming that the best control system will enforce an exact model following on the plant.

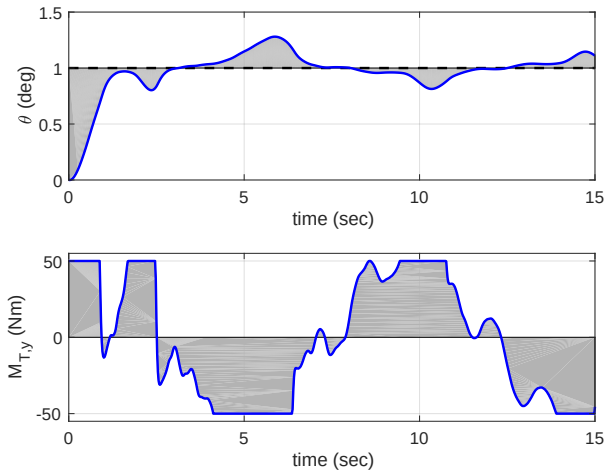

Figure 14. Controller performance indices: integrated control error (top) and control effort (bottom). The dashed line is the controller command.

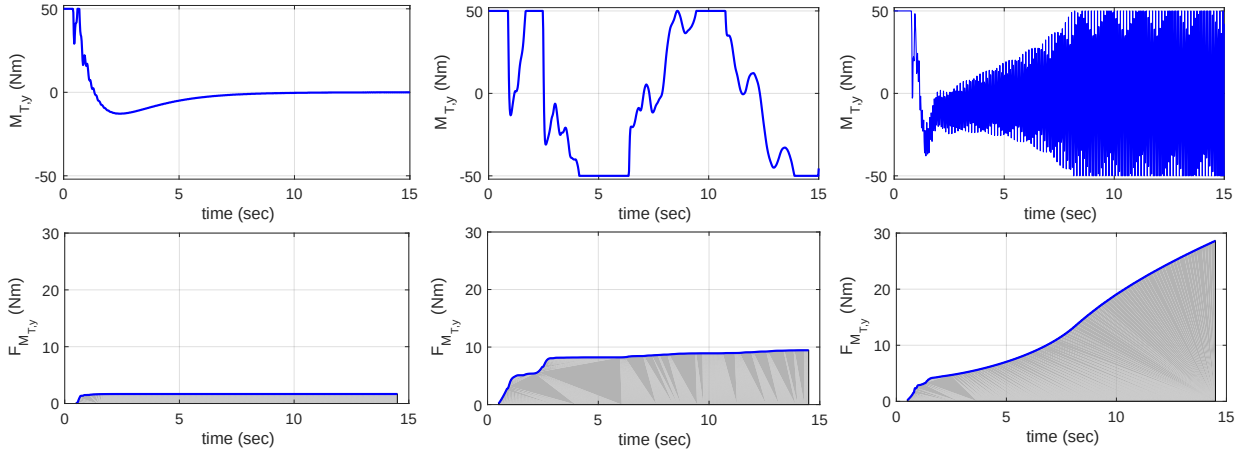

Figure 15. Actuator commands and cumulative standard deviation: nominal (left), off-nominal (middle), and unstable (right).

$$\sum_{\phi_{err}} = \int_0^t |\phi_c(t) - \phi_p(t)|\mathrm{d}t \qquad \sum_{\theta_{err}} = \int_0^t |\theta_c(t) - \theta_p(t)|\mathrm{d}t\ \phi \qquad \sum_{\psi_{err}} = \int_0^t |\psi_c(t) - \psi_p(t)|\mathrm{d}t \tag{24}$$

$$\sum_{M_{T,x}} = \int_0^t |M_{T,x}(t)|\mathrm{d}t \qquad \sum_{M_{T,y}} = \int_0^t |M_{T,y}(t)|\mathrm{d}t \qquad \sum_{M_{T,z}} = \int_0^t |M_{T,z}(t)|\mathrm{d}t \tag{25}$$

A graphic representation of the above metrics is shown in Fig. 14, represented by the grey areas, for a step command in the pitch angle when thruster control is used to follow this command. It is obvious that both individual areas should be as small as possible for optimal controller performance, which means they can be used to evaluate different controller designs. In the given example, $\sum_{\theta_{err}} = 1.738°$ s and $\sum_{M_{T,y}} = 523.3$ Nm s. Note that for the sake of this example the controller performance has been significantly downgraded (large pitch-rate gain for a satellite with very flexible solar panels).

To detect oscillations or otherwise discrete changes in the controls, the cumulative moving standard deviation can be used. For a subset j of n_s out of a total of N samples of an arbitrary control signal u,

the moving mean is defined as $\bar{y}_j = \frac{1}{n_s} \sum_{i=j}^{j+n_s-1} u_i$. Here, j will run from $j = 1+n_s/2$ to N-$n_s/2$, so each subsequent subset will shift by only one sample. Let the squared deviation from this mean be defined as $s_{u,j} = (u_{j+n_s/2} - \bar{y}_j)^2$, which represents the value at the midpoint of subset j. The cumulative standard deviation, F_u, for subset j is then

$$F_{u_j} = \sqrt{\frac{1}{N - n_s - 1} \sum_{k=1}^{j} s_k} \tag{26}$$

Figure 15 gives three examples of the behaviour of the pitch thrusters, given the step command of $\theta_c = 1°$. In the left two figures the pitch thruster activity is shown for the nominal response. Due to the discrete change in attitude command, the pitch thrusters exhibit a large jump in required control moment. This discrete jump contributes to a sudden increase in $F_{M_{T,y}}$. The corresponding (grey) surface under the curve, $\sum_{F_{M_{T,y}}} = \int_0^t F_{M_{T,y}}(t)\mathrm{d}t$, is a performance measure for these jumps, and should be as small as possible for smoother controls. For an off-nominal design case (the one shown in Fig. 14), where the controller performance has purposely been made worse, saturation periods can be discerned, as well as some low-frequency oscillations. Both effects result in a significant increase of $\sum_{F_{M_{T,y}}}$, although the effect of low-frequency oscillations is not that easy to spot. When in doubt, this criterion should be re-evaluated with different subset sample sizes, n_s. Finally, in the right-most two plots, the downgraded controller can no longer properly steer the satellite, and the actuator is rapidly oscillating between the minimum and maximum thrust values. These high-frequency oscillations are shown as a steady increase of $F_{M_{T,y}}$.

From these results it is obvious that by comparing the numerical values of $\sum_{F_{M_{T,y}}}$, conclusions can be drawn towards the control behaviour, even though it paints a *global* picture only. For the examples shown, these values are $\sum_{F_{M_{T,y}}} = 23.1$ Nm s, 113.2 Nm s and 191.1 Nm s, respectively. It may be clear that the *gradient* of $F_{M_{T,y}}$ is indicative of *local* oscillations. It is stressed, though, that the two parameters are indicative only, because both the choice of sample interval and the progression of the mean control value have an effect on the actual values. However, these performance metrics can serve their purpose in an automated procedure to optimise the control-system design.[d]

To link the controller performance to the flexible dynamics, an integrated panel deflection can be defined, or alternatively, the integrated motion of a single point (*e.g.,* the panel tip). Focussing on the former, the (absolute) motion of all structural nodes can be tracked over time, and similar to the performance indices defined earlier, three indices can be defined:

$$\sum_{u_x} = \int_0^t \int_0^L |u_x(\mathbf{x})|\mathrm{d}x\mathrm{d}t \qquad \sum_{u_y} = \int_0^t \int_0^L |u_y(\mathbf{x})|\mathrm{d}x\mathrm{d}t \qquad \sum_{u_z} = \int_0^t \int_0^L |u_z(\mathbf{x})|\mathrm{d}x\mathrm{d}t \tag{27}$$

where $u(\mathbf{x})$ is representing the (three-dimensional) displacement of a single node, the inner integral representing the total, absolute displacement of all nodes in the panel, and the outer integral determining the effect for the duration of the simulation. The subscripts x, y, and z indicate that the three vector components of the displacement vector are treated separately.

[d]That this is a useful criterion to include is shown by the following. Even though the thrusters are rapidly firing, the step response of θ is relatively smooth. Because the satellite is quite heavy (and inert), the rapidly switching bang-bang control will not result in a wild variation of θ; only the pitch rate exhibits a similar oscillation, albeit with small amplitude. So, if one would look at the control error only, $\sum_{\theta_{err}} = 2.769°$ s for the nominal case, and $\sum_{\theta_{err}} = 3.060°$ s for the oscillatory case, which is not significantly different. The integrated control effort *is* different, though: $\sum_{M_{T,y}} = 85.9$ Nm s (nominal) versus 402.7 Nm s (oscillatory). But, perhaps surprisingly, the second, off-nominal case has $\sum_{M_{T,y}} = 523.3$ Nm s, which is the highest of the three cases considered. Therefore, proper analysis of multiple aspects is recommended.

B. Controller Robustness

In general, the control-system design is started for a nominal system and mission, and once a satisfactory response performance is obtained the sensitivity to external perturbations is studied, as well as the uncertainties in the design parameters. And, depending on the level of fidelity of the analysis models used, modelling errors should be taken into account as well. Of course, given the perturbations the control system should still meet the requirements, in other words it should be robust, otherwise the control engineer would have a full-time job simply redesigning the controller every time the system design changes or new requirements about the perturbations come to light.

The potential advantage of adaptive control is that when a satellite design changes, its controller does not have to be redesigned without sacrificing performance and/or stability. Of course, these design changes should be within limits, one can think of, for instance, changes in mass properties and the "amount" of flexibility in the system. In this section the results of a sensitivity analysis after varying a number of the satellite's parameters are presented, a typical example of having a fast simulator at one's disposal during the conceptual design. The design-parameter variations have been selected quite arbitrarily, and are chosen to be large enough to have a noticeable effect. The following parameters are considered, given as a range around the nominal value:

(a) solar-panel geometry:

1. length, $L_{sp} = 14 \pm 4$ m ($\Delta = 30\%$)
2. width, $b_{sp} = 2.3 \pm 1.15$ m ($\Delta = 50\%$)
3. thickness, $t_{sp} = 0.03 \pm 0.015$ m ($\Delta = 50\%$)

(b) solar-panel mass and material:

4. mass, $m_{sp} = 40 \pm 20$ kg ($\Delta = 50\%$)
5. Young's modulus, $E_{sp} = (70 \pm 35) \cdot 10^9$ N/m^2 ($\Delta = 50\%$)
6. Shear modulus, $G_{sp} = (27 \pm 13.5) \cdot 10^9$ N/m^2 ($\Delta = 50\%$)

(d) satellite-bus geometry:

7. length, $L_{bus} = 2 \pm 1$ m ($\Delta = 50\%$)
8. width, $b_{bus} = 2.1 \pm 0.42$ m ($\Delta = 20\%$)
9. height, $h_{bus} = 2.8 \pm 0.56$ m ($\Delta = 20\%$)
10. link length, $L_{link} = 1.0 \pm 0.5$ m ($\Delta = 50\%$)

(d) satellite-bus mass and material:

11. mass, $m_{bus} = 1{,}950 \pm 380$ kg ($\Delta = 20\%$)
12. Young's modulus, $E_{bus} = (70 \pm 21) \cdot 10^9$ N/m^2 ($\Delta = 30\%$)
13. Shear modulus, $G_{bus} = (29 \pm 8.7) \cdot 10^9$ N/m^2 ($\Delta = 30\%$)

From the above parameters, several system parameters are derived, most notably the cross-sectional area, A, the area and polar moments, I_{yy}, I_{zz}, and J, and the average density, ρ:

$$A_{sp} = b_{sp} t_{sp} \qquad I_{yy,sp} = \frac{1}{12} b_{sp} t_{sp}^3 \qquad I_{zz,sp} = \frac{1}{12} b_{sp}^3 t_{sp}$$
$$J_{sp} = I_{yy,sp} + I_{zz,sp} \qquad \rho_{sp} = \frac{m_{sp}}{A_{sp} L_{sp}} \tag{28}$$

$$A_{bus} = b_{bus} h_{bus} \qquad I_{yy,bus} = \frac{1}{12} b_{bus} h_{bus}^3 \qquad I_{zz,bus} = \frac{1}{12} b_{bus}^3 h_{bus}$$
$$J_{bus} = I_{yy,bus} + I_{zz,bus} \qquad \rho_{bus} = \frac{m_{bus}}{A_{bus} L_{bus}} \tag{29}$$

These parameters, as well as the material properties, E and G, enter the matrices Eqs. (10) and (11), at the appropriate places for the elements associated with solar panel, satellite bus, and link.

The controller analysis is centred around a single manoeuvre, *i.e.,* combined step commands of $\phi_c = \psi_c$ = 1° and θ_c = -1° executed at t = 0 s, identical to the one discussed in Sec. II.C. The adaptive-controller response for a rigid satellite is shown in Fig. 4. Figure 5, on the other hand, shows the control errors for both controllers, *i.e.,* the LQR and the SAC. The nominal response of both controllers for a satellite with flexible panels is quite similar to the one for the rigid satellite, and will not be shown again. However, to have a baseline performance, the following values of the performance indices discussed in the previous section are found, first for the SAC and in between brackets for the LQR. It is noted that the controller designs are those as discussed in Secs. II.B and II.C for the LQR and SAC, respectively.

- Control error: $\sum_{\phi_{err}}$ = 2.96 (2.71)° s, $\sum_{\theta_{err}}$ = 2.71 (2.73)° s, $\sum_{\psi_{err}}$ = 3.10 (2.79)° s.
  The integrated control errors are relatively small and comparable for both controllers, with slightly smaller values for the LQR (apart from θ_{err}). Characteristic for the SAC is that, if not properly tuned, the controller is a bit slower to start, but shows a more stable response in the long run. With the right set of weights, the LQR is known for its rapid and smooth transient response for the nominal configuration it is designed for.

- Control effort: $\sum_{M_{T,x}}$ = 29.9 (24.5) Nm s, $\sum_{M_{T,y}}$ = 79.2 (86.6) Nm s, $\sum_{M_{T,z}}$ = 89.2 (86.1) Nm s.
  Both controllers saturate when the step is applied, but for ϕ_c and ψ_c the LQR uses less fuel to reach steady state. This is not true for θ_c, though, where the SAC is more efficient. During preliminary runs it was found that the y-axis is more difficult to control, and the SAC seems to be (marginally) better prepared for this task.

- Oscillatory behaviour: $\sum_{F_{M_{T,x}}}$ = 25.4 (18.2) Nm s, $\sum_{F_{M_{T,y}}}$ = 16.2 (26.9) Nm s, $\sum_{F_{M_{T,z}}}$ = 46.7 (18.6) Nm s.
  Even though there are somewhat larger differences, the response is comparable. This performance index is also affected by a discrete change in control moment – as discussed previously – and the SAC shows more discrete changes, because of the larger gains. Despite that, for the y-axis it performs smoother than the LQR, which may indicate that the y-axis is posing more of a problem to the LQR than the x- and z-axes.

- Integrated panel deflection: $\sum_{u_x}$ = 0.087 (0.087) m s, $\sum_{u_y}$ = 2.601 (2.650) m s, $\sum_{u_z}$ = 2.685 (2.660) m s.
  The integrated deflection is quite an abstract parameter that may be difficult to interpret. This is a measure of sustained duration away from an initial (or desired) position, also known as absement. It will be used for a relative comparison between the configurations rather than an absolute one. Typically, a larger value means more motion of the solar panel, possibly induced by discrete jumps in the control moments. Therefore, one desires a small value for absement also, although, it is possible for the satellite bus to be controlled with non-constant absement through the symmetric motion of the solar panels. For the nominal configuration, both SAC and LQR show more or less the same flexible behaviour.

Now that the baseline performance has been established, a Monte-Carlo batch of simulations is performed. For a total of 500 satellite configurations, the 13 design parameters are sampled according to a uniform distribution. Each configuration is simulated with both the SAC and the LQR (with an identical random sequence of design parameters, such that the performance can be compared), and the performance indices are evaluated per run. In Figs. 16 through 20 the resulting histograms are shown, in relation to the nominal configuration. These will now be briefly discussed.

Figure 16 shows the control error (or integrated state deviation). In spite of the large variation in design parameters, both controllers do an excellent job to keep the control error limited and centred around the nominal performance. The LQR exhibits superior performance in that respect, with not only a smaller error, but also with less variation. The slightly larger error for the SAC (between 10-15%) has been explained before and the same reasoning holds now. Concerning the y-rotation and the fact that this axis is more difficult to control, the results are acceptable. The SAC has a larger variation than the LQR, with in absolute sense some smaller and some larger errors than the LQR. Concluding, for this particular manoeuvre the controller performance is good.

The control effort (Fig. 17), on the other hand, suggests greater differences. The x-thruster activity is similar for both controllers and centred around the nominal configuration (which is about 20% larger for

the SAC), albeit the LQR has an outlier around 45 Nm s. The nominal performance of the z-thruster is almost the same, and the distributions are almost overlapping. The y-thruster, on the other hand, has three outliers far away from the nominal configuration. This seems to indicate an excessive thruster use. This is confirmed by Fig. 18, where the oscillatory behaviour of the thrusters is shown. The y-thruster has indeed the "same" three outliers, indicating strong oscillations, which would also explain the large control effort.

Isolating the individual run with the strongest oscillations from the results is easy, and inspecting the actual angle and thruster history indicates what happens. In Fig. 19 the related curves are shown. Indeed, the pitch thruster is wildly oscillating and basically exhibits a bang-bang control at the controller frequency. Surprisingly, the attitude remains stable, but fuel is, of course, depleted quickly in this way. Somehow, these oscillations seem to transfer into the x and z control as well, indicated by the high-frequency oscillations, albeit with small amplitude. In any case, high-frequency actuator switching should be absolutely avoided. As a matter of fact, these small-amplitude oscillations in x and z do not show up in $F_{M_{T,x}}$ and $F_{M_{T,z}}$, which means that one should not rely on a single performance index. And, when in doubt, inspect the individual time histories of selected variables.

The adaptive controller seems to handle this particular satellite configuration well, judging from the absence of any oscillations, not only for this run, but for the other outliers of the y-thruster as well. The distribution of $F_{M_{T,z}}$ is shifted to the right of the histogram, though, but as was discussed earlier, any discrete actuator change also contributes to $F_{M_{T,z}}$. And that is also observed in Fig. 19, where the z-thruster experiences some "ragged" commands. This may have to be studied in more detail, but for now it is safe to conclude that the adaptive controller is more robust towards design changes in the satellite.

The high-frequency oscillations do not seem to have an adverse effect on the flexible motion. Figure 20 shows the integrated beam deflection, which appears similar for both controllers. The x- and y-directions exhibit a stronger deflection for the LQR, which might indeed be oscillation-induced. The z-deflection is a little higher for the SAC, but it was already observed that the z-direction is more difficult to control for the SAC. The total variation of these indices (between 30-50%) does not seem unrealistic, considering the equally large variations in E and G. This could potentially lead to the conclusion that the controllers do not induce additional, unwanted flexible-panel motion.

C. Controller Design

In the previous section it was shown that the LQR has a better performance for the nominal satellite configuration. In this section, another use of the simulation environment is explored, namely that of controller design. The initial design parameters of the adaptive controller were selected rather arbitrarily, and manually tuned until a reasonable response was obtained. The full potential of the design was not explored, though, but on the other hand, if all design parameters would have been included the design process would have taken unacceptably long. What is meant here is that asymmetric, full weighting matrices could have been used, as well as non-zero values for all initial integral gains. Usually not required, but it could come in handy

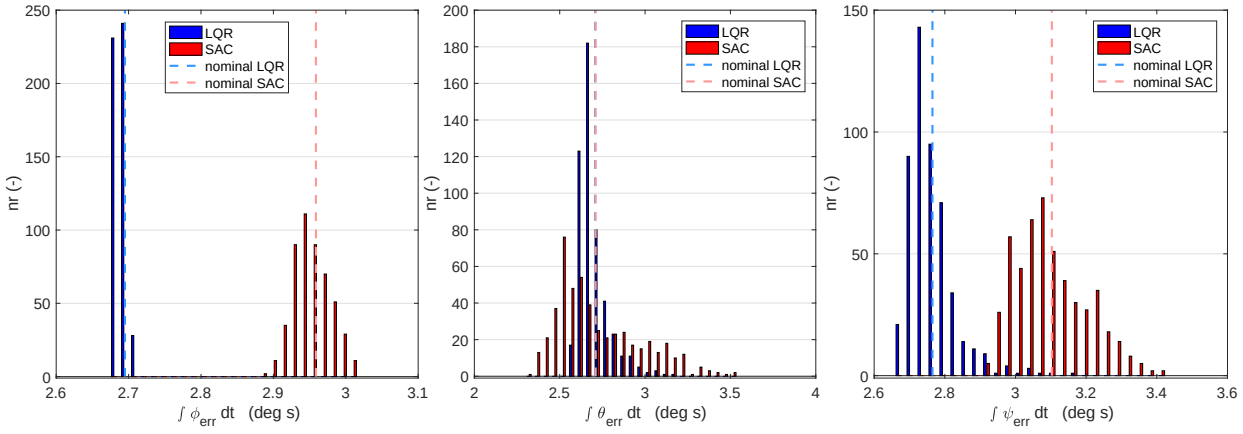

Figure 16. Integrated control errors for varying satellite configurations (combined step commands).

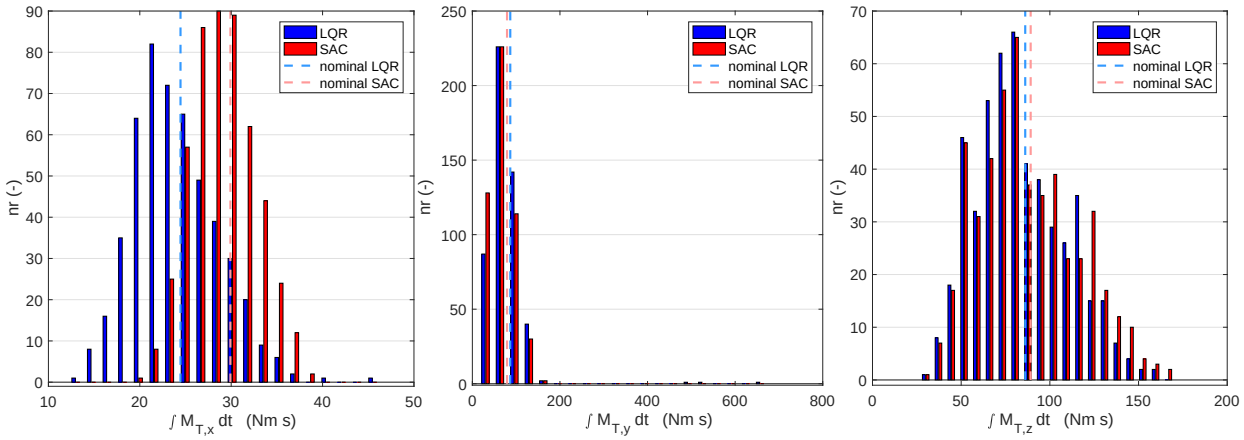

Figure 17. Integrated control effort for varying satellite configurations (combined step commands).

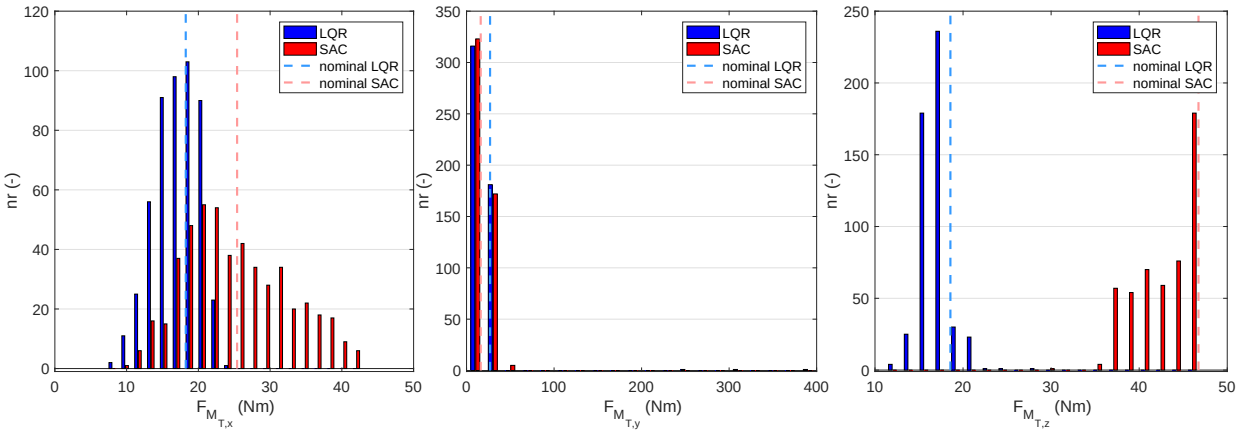

Figure 18. Oscillatory behaviour for varying satellite configurations (combined step commands).

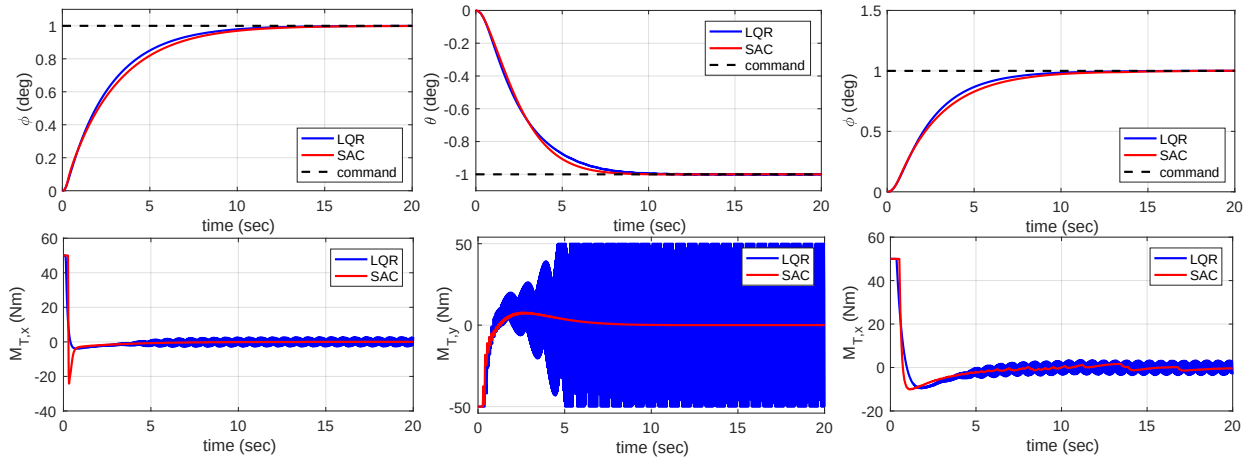

Figure 19. Unstable actuator behaviour for LQR (combined step commands).

for systems that are more difficult to control. To be fair, it is surprising to see the excellent performance of the LQR in most situations, with a design process that is a lot easier and shorter than for the SAC. But, in

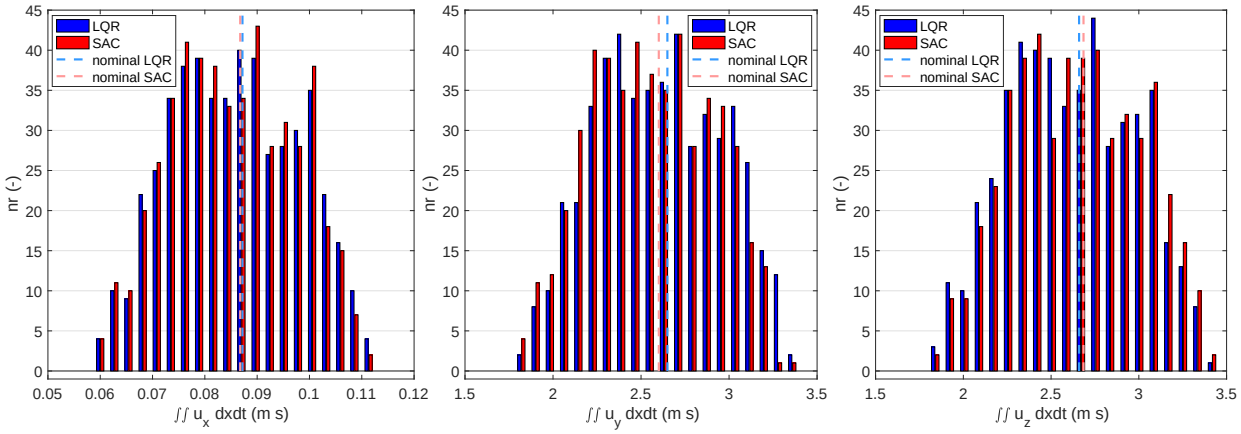

Figure 20. Integrated panel deflection for varying satellite configurations (combined step commands).

case robustness becomes a design driver, the LQR falls short.

Without going to great length, in this section the variation of the design parameters of the SAC is discussed as an example of performance improvement by design. The nominal satellite configuration introduced in the previous section is used, and the controller design parameters are varied in a similar manner as was the satellite configuration. The design parameters to be considered are taken from Tables 1-3, where the listed values are nominal. Each parameter is varied over a ±50% range. The total number of design parameters is 36, being:

(a) roll controller:

1-8. weighting matrices $\mathbf{T_p}$ and $\mathbf{T_i}$: diagonal elements related to e_ϕ, p_m, ϕ_m, $M_{Tm,x}$

9-12. integral-gain initial value: $K_{i,0}$ related to e_ϕ, p_m, ϕ_m, $M_{Tm,x}$

13. integral-gain filter constant: σ_i related to e_ϕ

(b) pitch controller:

14-21. weighting matrices $\mathbf{T_p}$ and $\mathbf{T_i}$: diagonal elements related to e_θ, q_m, θ_m, $M_{Tm,y}$

22. integral-gain initial value: $K_{i,0}$ related to e_θ

23. integral-gain filter constant: σ_i related to e_θ

(c) yaw controller:

24-31. weighting matrices $\mathbf{T_p}$ and $\mathbf{T_i}$: diagonal elements related to e_ψ, r_m, ψ_m, $M_{Tm,z}$

32-35. integral-gain initial value: $K_{i,0}$ related to e_ψ, r_m, ψ_m, $M_{Tm,z}$

36. integral-gain filter constant: σ_i related to e_ψ

A total of 1,000 simulations are performed, and the same performance indices as before are evaluated. A subset of the results has been summarised in Figs. 21 and 22. It is noted that doing a Monte-Carlo analysis to improve the controller performance is far from optimal, let alone efficient. In older research it was shown that using, for instance, an evolutionary algorithm gives better results at far less computational cost.[16] With the relatively fast framework developed in this paper such an optimisation method is certainly within reach.

Figure 21(a) indicates that the performance of the LQR ($\sum_{\phi_{err}} = 2.71°$ s and $\sum_{M_{T,x}} = 24.5$ Nm s) is not met, although the nominal performance has improved between 1-3%. The nominal performance of the pitch thruster was already better than the LQR, and has improved a bit more, about 3-4%. Interesting to see is that there is a significant number of controller designs with a better performance. Considering the performance of the the yaw thruster (LQR: $\sum_{\psi_{err}} = 2.79°$ s $\sum_{M_{T,z}} = 86.1$ Nm s), the control error has dropped

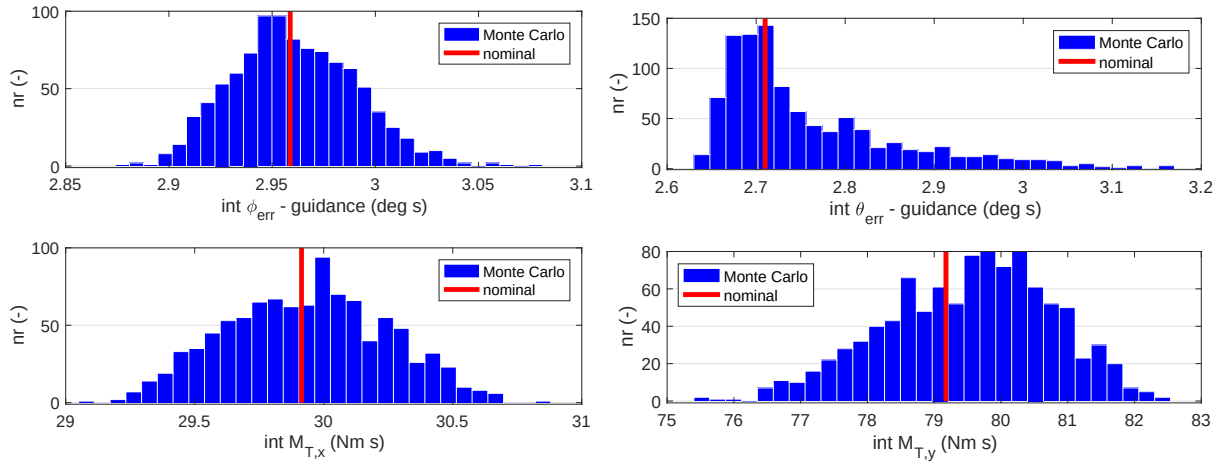

(a) Roll

(b) Pitch

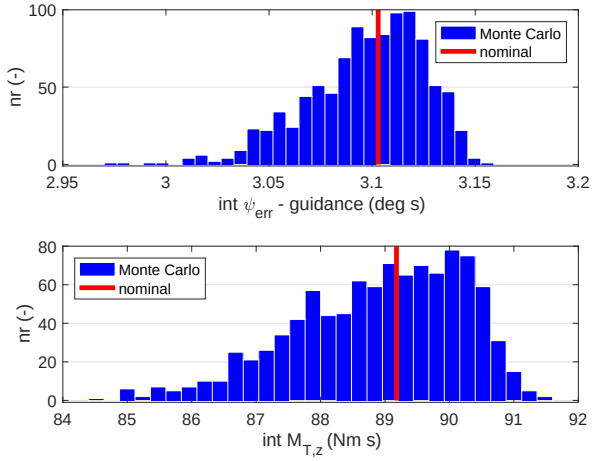

(c) Yaw

Figure 21. Adaptive-controller redesign: integrated control errors and control effort (combined step commands).

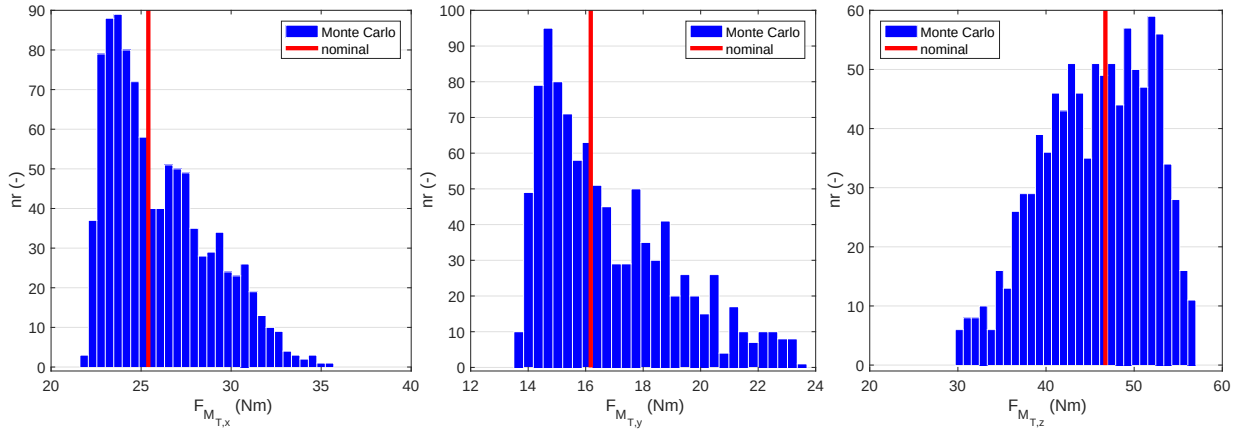

Figure 22. Adaptive-controller redesign: oscillatory actuator behaviour (combined step commands).

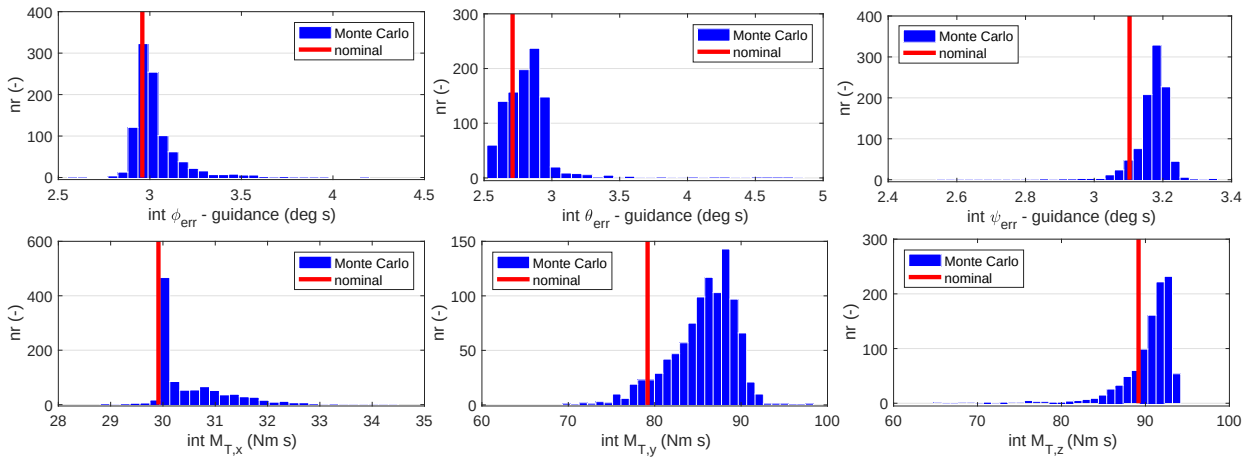

Figure 23. Adaptive-controller extended design range: controller performance (combined step commands).

to value just above the LQR one, but the control effort has dropped slightly below the LQR value (the minimum value is now $\sum_{M_{T,z}} = 84.5$ Nm s). The oscillatory behaviour of the controls shows a more significant improvement (Fig. 22). Even though the values for roll and yaw control do not go below the ones for the LQR, the improvement for the yaw thruster is over 30% (roll thruster: about 12%). The pitch thruster, which was already more stable than its LQR counterpart, has reduced from $\sum_{F_{M_{T,y}}} = 16.2$ Nm s to 13.8 Nm s.

It remains to be studied whether the performance indices reduce simultaneously, but this brief analysis has shown that with the current simulation environment and approach, the controller performance can be analysed and improved, where necessary. To show the limitations of a Monte-Carlo variation of the design parameters instead of a proper optimisation process, a final Monte-Carlo batch is run where the controller parameters are varied between 5-400% of their nominal values (1,000 runs). Results for the control errors and control effort are shown in Fig. 23. In general, the performance has degraded, as the parameter variation is apparently too large and possibly some of the parameters are dominating the response. However, there are actually a few runs that approach the LQR performance or are even better.

Looking at just the minimum values of the performance indices shows that in almost all of the indices *a* controller configuration can be found that has a better performance than the LQR. Unfortunately, none of these configurations are the same, so undoubtedly a compromise has to be found based on specific requirements. Alternatively, one can also optimise the individual controllers separately, since the motion axes are largely decoupled. In that case, with fewer design parameters per batch, convergence is expected to be relatively quick. Summarised, the following minimum values are obtained:

- Minimum control error: $\sum_{\phi_{err}} = 2.56\ (2.71)^\circ$ s, $\sum_{\theta_{err}} = 2.54\ (2.73)^\circ$ s, $\sum_{\psi_{err}} = 2.54\ (2.79)^\circ$ s. All minimum errors are now below the LQR values.
- Minimum control effort: $\sum_{M_{T,x}} = 28.8\ (24.5)$ Nm s, $\sum_{M_{T,y}} = 69.5\ (86.6)$ Nm s, $\sum_{M_{T,z}} = 65.2\ (86.1)$ Nm s. Roll thruster effort has reduced, but is a little above the LQR performance. Both pitch and yaw thruster are well below the LQR nominal values.
- Minimum oscillatory behaviour: $\sum_{F_{M_{T,x}}} = 20.0\ (18.2)$ Nm s, $\sum_{F_{M_{T,y}}} = 13.3\ (26.9)$ Nm s, $\sum_{F_{M_{T,z}}} = 12.1\ (18.6)$ Nm s. The roll thruster oscillatory behaviour has dropped about 20%, but is still a bit above the LQR value. The pitch thruster value is half the LQR one, and the yaw thruster has become "more stable" by about 70% (from 46.7 down to 13.3 Nm s) and has now a value lower than the LQR.

VI. Conclusions and Recommendations

A simplified three-dimensional beam model was created, which precluded a complicated interactive system of rigid and elastic bodies coupled through force (Lagrange) multipliers. However, the commercial beam model was superior to the simplified model that has been developed, albeit at a very high computational cost. Therefore, it is impractical to use the commercial model with such rapidly changing system states and applied loads. One can conclude that the linear beam model is a reasonable first-order estimate for the controller design. It should be noted that it performs much faster than complex nonlinear models and is suitable to rapidly develop adaptive gains for the simple adaptive controller. The intention is also not to replace the more accurate models with a simplified beam model, but to first generate the performance values and adaptive gains, before continuing the structural dynamic analysis with a more complicated, and more computationally expensive, model.

Performance indices were evaluated for three characteristics: the Euler-angle deviation, the integrated thruster activity, and the integrated panel deflection. The first two indices gauged the global performance of the controller by comparing the minimum state deviation of the satellite with respect to guidance commands and comparing the minimum control effort that is required to influence the behaviour of the plant. The third index linked the performance of the controller with the flexible dynamics, as the absolute motion of all the structural nodes were tracked over time and integrated, representing the directional absement of the solar panels. This gave an indication of the vibration or motion of the panels with respect to the satellite bus. In certain cases, the performance of the controllers based on only one index did not suggest controller instability; however, with the combination of at least one other index it became clear that the SAC was stable, but the linear quadratic regulator was unstable.

The robustness of the two controllers, LQR and SAC, was examined by varying the geometric and mechanical parameters of the satellite system. The variation of the system parameters was up to 50%, but was performed with respect to a single manoeuvre of three combined step commands of 1 deg executed immediately at simulation start. The baseline characteristics were that the SAC had a slow start with regards to the control error, but was more stable in the long run. The LQR, known for its rapid and smooth transient response performed better and used less fuel for the steady state, although it had more difficulty controlling the y-axis.

For the Monte-Carlo simulations, both controllers limit control error, but the LQR outperformed the SAC in terms of inducing smaller errors, but also with less deviation. The simple adaptive controller also had more difficulty in controlling the z-deflections. However, in terms of control effort, the SAC generally performed as well as the LQR for x-thruster and slightly poorer for z-thruster activity, but the LQR had three outlying cases for the y-thruster control effort. This indicated unstable behaviour of the LQR for certain combined commands, which were handled well by the SAC.

A Monte-Carlo-based adaptive controller design was also introduced; although the full potential of the design was not explored, the relatively fast framework developed in this paper allowed the improvement of the SAC performance. While the performance of the LQR is still not objectively always met, the nominal performance of the simple adaptive controller was improved by 1-3%. The pitch thruster performance, which was already better than the LQR, improved between 3-4%. There were a significant number of adaptive controller designs with better performance. After optimisation using the Monte-Carlo design, the minimum control errors fell below all those of the LQR, the minimum control effort was reduced; although the roll thruster had reduced effort, it was still above the LQR performance, despite the pitch and yaw thruster efforts well below that from the LQR. The oscillatory behaviour is lower than the LQR, except for the roll thruster, but still improved by 20%. The pitch thruster oscillation is less than half that from the LQR, and the yaw thruster is more stable and about two-thirds the LQR value.

Some of the future work will revolve around the improvement of the beam model, without resorting to higher-complexity models, and determining the robustness of a nonlinear model that will allow the development of larger rotations than the current linear model. Such a nonlinear model would be useful to compare with a fully nonlinear continuum model, which was presented in previous works by the authors. Also the use of a Runge-Kutta integration should be considered to reduce the numerical issues. With a model that can accurately incorporate large rotations, one could examine more complex manoeuvres and develop control strategies for capture operations, faster autonomous manipulator movement, or collision avoidance with orbital debris. With respect to controller design, the performance-optimisation methodology should be further developed, and linked with actual design requirements.

References

[1]Mooij, E. and Wijnands, Q.G.J., "Real-Time Implementation of a Model Reference Adaptive Control System", AIAA-2003-5754, *AIAA Simulation and Modelling Technologies Conference*, Austin, TX, August 11-14, 2003.

[2]Gransden, D., Bornemann, P. B., Rose, M., Nitzsche, F., "A Constrained Generalised-α method for coupling rigid parallel chain kinematics and elastic bodies", *Journal of Computational Mechanics*, Vol. 55, 2015, pp. 527-541.

[3]Gransden, D.I. and Mooij, E., "Simple Adaptive Control of a Satellite with Large Flexible Appendages", IAC-16-C1.8.8.x35217, *67th International Astronautical Congress*, Guadalajara, Mexico, September 26-30, 2016.

[4]Kaufman, H., Barkana, I. and Sobel, K., *Direct adaptive control algorithms: Theory and applications*, Second edition, Springer-Verlag, New York, 1998.

[5]Mooij, E., "Passivity Analysis for Non-Linear, Non-Stationary Entry Capsules", *Int. J. Adapt. Control Signal Processing*, Published Online 2013.

[6]Gopal, M., *Modern Control System Theory*, Wiley Eastern Ltd., New Delhi, Second Reprint, June 1989.

[7]Gili, P. *et al.*, "Articulated and Flexible Multibody Satellite Dynamics Modelling", AIAA-2002-2056, *20th AIAA International Communications Satellite Systems Conference and Exhibit*, 2002.

[8]Zhang, M.-J., and Zhao, C.-Y., "Attitude stability of a spacecraft with two flexible solar arrays on a stationary orbit around an asteroid subjected to gravity gradient torque", *Astrophysics Space Science*, Vol. 351, 2014, pp. 507-524.

[9]Gasbarri, P., Monti, R., Sabatini, M., "Very large space structures: Non-linear control and robustness to structural uncertainties", *Acta Astronautica*, Vol. 93, 2013, pp. 252-265.

[10]Gasbarri, P., Monti, R., De Angelis, C. Sabatini, M., "Effects of uncertainties and flexible dynamic contributions on the control of a spacecraft full-coupled model", *Acta Astronautica*, Vol. 94, 2014a, pp. 81-97.

[11]Gasbarri, P., Sabatini, M., Leonangeli, N., and Palmerini, G., "Flexibility issues in discrete on-off actuated spacecraft: Numerical and experimental tests", *Acta Astronautica*, Vol. 101, 2014b, pp. 515-526.

[12]Simeon, B., "On Lagrange multipliers in flexible multibody dynamics",*Computational Methods in Applied Mechanical and Engineering*, Vol. 195, 2006, pp. 6993-7005.

[13]Ferreira, A. J. M., "MATLAB Codes for Finite Element Analysis: Solids and Structures", Springer, Dordrecht, The Netherlands, 2009.

[14]Oñate, E., *Structural analysis with the finite element method. Linear statics: volume 2: beams, plates and shells*, Springer Science & Business Media, 2013.

[15]Gransden, D.I., and Mooij, E., "Control Recovery of a Satellite with Large Flexible Appendages after Impact", AIAA-2018-2099, *AIAA SciTech Forum: AIAA/AAS Space Flight Mechanics Meeting*, Kissimmee, FL, 8-12 January 2018.

[16]Mooij, E., "Evolutionary Optimisation of a Model Reference Adaptive Control System", AIAA-2002-4922, *AIAA Guidance, Navigation, and Control Conference*, Monterey, CA, August 5-8, 2002.